Vibrational Förster transfer in ice Ih

R. L. A. Timmer,* and H. J. Bakker

FOM-institute for Atomic and Molecular Physics, Kruislaan 407, 1098 SJ Amsterdam, The Netherlands

E-mail: r.timmer@amolf.nl

Abstract

We have studied Förster energy transfer between O–H vibrations in H_2O/D_2O ice Ih using femtosecond, two-color, mid-infrared pump-probe spectroscopy. We find that as a result of couplings to nearby O–H stretch modes, the vibrational relaxation time decreases from 480 fs for dilute HDO in D_2O down to 300 fs for pure H_2O ice. The anisotropy shows an initial 140 fs decay down to a concentration dependent end level. This end level for low concentrations can be explained from the limited rotational freedom ($\sim$20°) of a water molecule in the ice lattice over time scales $>$15 ps. The decreasing end levels for higher concentrations of H_2O result from Förster energy transfer to the next nearest six O–H groups. No Förster transfer beyond these neighbors is observed. Variation of the ice temperature between 200 and 270 K was found to have negligible effect on the dynamics.

Introduction

Hexagonal ice Ih is the most common form of ice found on earth. Its hexagonal structure is just one of more than a dozen different polymorphs currently known. In the structure of ice Ih, the oxygen atoms lie on a hexagonal 'wurtzite' lattice (symmetry C_{6h}, space group $P6_3/mmc$).[1] Different

polymorphs may vary in crystalline structure, ordering and density, but the water molecule is always hydrogen bonded to four neighbors in a tetrahedral arrangement. There are six different arrangements of the two hydrogen atoms of water over these four neighbors, leading to six different orientations. In ice Ih these orientations are randomly ordered, subject to the so called Bernal-Fowler ice rules.[2] These state that each oxygen atom is connected to two nearby hydrogen atoms and that on each connection between two oxygen atoms, exactly one hydrogen resides.

Energy relaxation in liquid water and ice consists of both intra- and intermolecular energy transfer[3–5] pathways. In general, the dissipation rate of (vibrational) energy depends on the number density and coupling strength of accepting modes that are present in proximity to the excited oscillator. In liquids, such as water, the frequencies of these modes are continuously modulated through variations in the hydrogen bond distance, strength and angle.[6,7] In comparison to water, the structure of ice is much more rigid and the molecules form nearly homogeneous hydrogen bond connections with all four of their neighbors at directions close to the tetrahedral angle (109.5°). This tetrahedral arrangement causes the open structure of ice Ih and explains its relatively low density compared to water (0.92 g/cm^3 vs 1.00 g/cm^3).

Long-range intermolecular energy transfer between molecules is possible through a direct dipole-dipole coupling mechanism, called Förster energy transfer.[8] A technique well suited for the study of this energy transfer on the sub-picosecond timescale is polarization-resolved pump-probe spectroscopy.[9–14] The preferential absorption of polarized light along the direction of the vibrational transition dipole moment axis can be used to track the changing direction of the excitation that results from either reorientational diffusion[4,14,15] or Förster energy transfer between modes located on differently oriented (water) molecules. Because the molecules in ice are expected to exhibit only limited reorientational diffusion, we expect that the main mechanism for a change in the direction of the excitation will be vibrational Förster energy transfer.

Due to its simple and ordered structure, ice provides an ideal environment in which to test different theoretical models of the water molecule, such as those concerning dipole-dipole interactions and vibrational energy transfer. Previous studies using polarization-resolved spectroscopy

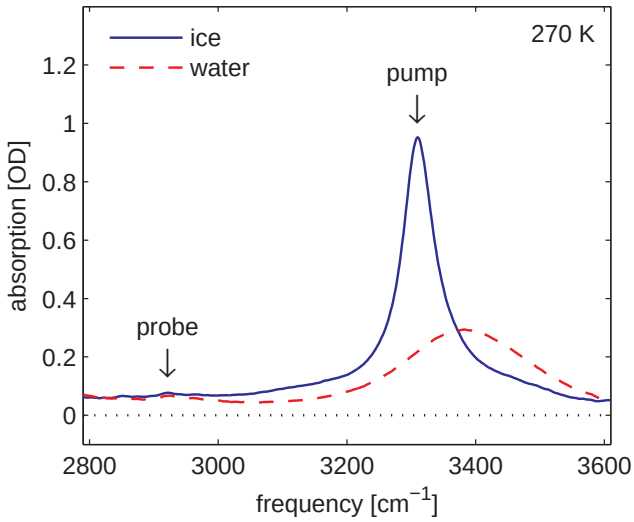

Figure 1: Linear absorption spectra of the O–H stretch vibration in ice and water (f_H=2%). The arrows indicate the pump and probe frequencies used in the experiments. The pump coincides with the $v = 0 \rightarrow 1$ transition (3310 cm^{-1}) and the probe with the $v = 1 \rightarrow 2$ induced absorption (2925 cm^{-1}).

found that the rate of vibrational Förster transfer between O–H oscillators in liquid water occurs on sub 100 fs timescales.[16,17] Here we study these dynamics for the O–H stretching mode in ice, using various mixtures of normal (H_2O) and heavy (D_2O) water. Thereby we vary the density and thus the average distance between O–H oscillators in the ice lattice.

Experimental section

Samples consisted of mixtures of normal water (H_2O) and heavy water (D_2O) with the fraction of hydrogen,

$$f_H = \frac{[H_2O]}{[H_2O]+[D_2O]} = \frac{H}{H+D}, \quad (1)$$

varying between 0.1 and 100%. The samples were frozen using a closed-circuit liquid helium pumped cryostat (temperature stability 0.5 K). The freezing procedure consisted of a rapid (few minute) cool down to 250 K, until the sample showed a homogenous ice crystal. The sample temperature was then set to 270 K and a series of linear spectra was taken before, during and after

the experiment to confirm that the sample remained frozen (see Figure 1).

The experiments were performed using a femtosecond, two-color, mid-infrared pump-probe laser setup. A commercial Ti:Sapphire system (Quantronix Titan) delivered pulses with a central wavelength of 800 nm at a repetition rate of 1 kHz. This light was split in three parts. Two parts were used to pump two separate BBO based Optical Parametric Amplifiers (OPA). The idler pulses from the first OPA were doubled and combined with the third 800 nm part in a parametric amplification process in a Potassium Titanyl Phosphate (KTP) crystal to yield 150 fs pump pulses at a frequency of 3310 cm^{-1}. Signal and idler pulses from the second OPA were recombined using a difference-frequency mixing process in a $AgGaS_2$ crystal to yield 150 fs probe pulses at a frequency of 2900 cm^{-1}. The pump and probe pulses had pulse energies of 5 μJ and 20 nJ, respectively. The instrument response time was about 200 fs.

The probe was split into two beams by reflection off a CaF_2 wedged window. One of these beams was overlapped with the pump beam in the sample while the other was used as a reference beam to compensate for intensity fluctuations in the individual laser pulses. The delay time t between pump and probe was varied by means of a delay stage with a resolution of 0.03 ps. The pump and probe beams hit the sample with a relative difference in polarization angle of 45 degrees. After the sample, the probe beam was sent onto a rotating polarizer, which alternately selected between polarization components parallel ($\Delta\alpha_{\parallel}$) and perpendicular ($\Delta\alpha_{\perp}$) to the pump beam. The probe and reference beams were frequency resolved (ν) by a polychromator and detected by two 32-pixel Mercury Cadmium Telluride (MCT) arrays. The pump beam was modulated with a 500 Hz chopper to distinguish only the pump induced absorption changes.

The absorption cross section of infrared active modes, such as the O–H stretch vibration, is proportional to the directional overlap between the transition dipole moment of the absorbing oscillator and the polarization of the light. In this experiment the pump beam, which is linearly polarized, excited an anisotropic population of O–H stretch modes from the vibrational ground state $\nu = 0$ to the first excited state $\nu = 1$. The absorption differences, caused by this excitation

may be split in to isotropic ($\Delta\alpha$) and anisotropic (R) parts using:[18]

$$\Delta\alpha(t,\nu) = \frac{\Delta\alpha_{\parallel}(t,\nu)+2\cdot\Delta\alpha_{\perp}(t,\nu)}{3}, \quad (2)$$

$$R(t,\nu) = \frac{\Delta\alpha_{\parallel}(t,\nu)-\Delta\alpha_{\perp}(t,\nu)}{\Delta\alpha_{\parallel}(t,\nu)+2\cdot\Delta\alpha_{\perp}(t,\nu)}. \quad (3)$$

The isotropic signal depends only on the vibrational excitation and is independent of its direction. Conversely, the anisotropy R is proportional to the auto-correlation function of the direction of the excitation:

$$R(t) = {}^{2}/_{5}\,\langle P_2(\hat{\mu}(0)\cdot\hat{\mu}(t))\rangle \quad (4)$$

where $\hat{\mu}(0)\cdot\hat{\mu}(t)$ is the inner product between unit vectors along the direction of transition dipole moments at times 0 and t. P_2 is the second Legendre polynomial and $\langle ...\rangle$ denotes the ensemble average.

Depopulation of the ground state leads to a reduced absorption or 'bleach' at frequencies corresponding to the $\nu = 0 \rightarrow 1$ transition. This reduced absorption is enhanced by $\nu = 1 \rightarrow 0$ stimulated emission of the excited population back to the ground state. At the same time the newly created population in the first excited state $\nu = 1$ starts to absorb light at frequencies that correspond to the $\nu = 1 \rightarrow 2$ transition. For anharmonic oscillators, such as the O–H stretch vibration, the energy spacing between the levels goes down with increasing quantum number. This means that the $\nu = 1 \rightarrow 2$ transition lies at a lower frequency than the $\nu = 0 \rightarrow 1$ transition.

Here we pump the $\nu = 0 \rightarrow 1$ transition and probe the $\nu = 1 \rightarrow 2$ induced absorption. There are several advantages to this approach:

- Although the ice crystal appeared optically clear, we experienced considerable scatter light of the pump beam in the direction of the probe. Detection of this scattered light can be avoided by probing at a different frequency than the pump.

- In a previous study on the transient absorption spectrum of ice Ih,[5] it was shown that the decay of the excited state occurs through a blue-shifted intermediate level. The spectrum

of this intermediate level complicates the analysis of the anisotropy and can be avoided by probing the $\nu = 1 \rightarrow 2$ absorption.

- For samples containing higher concentrations of H_2O, the optical density was such that hardly any probe light was transmitted in the region of the $\nu = 0 \rightarrow 1$ absorption. This problem is not present in the region of the $\nu = 1 \rightarrow 2$ induced absorption. In addition, the narrowing of the O–H absorption peak upon freezing of the sample was helping to clear the probing region.

- For the reorientation of the O–H in liquid water it was shown[15] that the anisotropy in the frequency region of the $\nu = 0 \rightarrow 1$ absorption may be distorted by a slightly faster reorientation of excited molecules during their relaxation compared to unexcited molecules. This higher mobility ultimately leads to the creation of an anisotropic orientational distribution of O–H groups in the ground state. The effect is thus only present for the ground state ($\nu = 0 \rightarrow 1$) absorption spectrum does not influence the dynamics at the $\nu = 1 \rightarrow 2$ frequency.

From the isotropic signal we obtain information about the vibrational relaxation rate k which depends on the density and cross-section of nearby accepting modes. The anisotropic signal reveals information about reorientational motion (or lack thereof) and vibrational Förster transfer. Using Eq. 4, it can be shown[18] that the anisotropy that results from the uniform reorientational diffusion of an excitation within a cone of half-angle θ_r equals:

$$R_{\text{cone}} = {}^{2}\!/_{5} \left({}^{1}\!/_{2} \cos(\theta_r) \cdot [1 + \cos(\theta_r)] \right)^2 . \tag{5}$$

The anisotropy that results from an excitation that changes direction over an angle θ_t as a result of energy transfer, equals:[18]

$$R_{\text{transfer}} = {}^{1}\!/_{5} \left(3 \cos(\theta_t)^2 - 1 \right) . \tag{6}$$

Both reorientation and Förster transfer contribute to the decay of the anisotropy. By decreasing the fraction of O–H groups in the sample (f_H), we can limit the anisotropy decay as a result of Förster

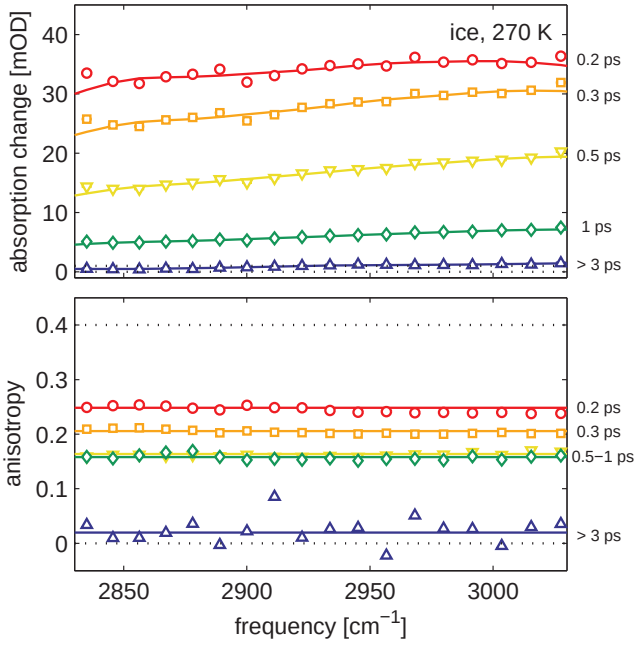

Figure 2: Transient absorption spectra of 15% H_2O ice at various delays between pump and probe. The probe region shows part of the $\nu = 1 \rightarrow 2$ induced absorption which for ice Ih is unusually broad[5] (2700-3300 cm^{-1}). The isotropic signal (top) shows a quick decay to a small end spectrum (> 3 ps). The anisotropy (botton) shows a frequency independent rapid initial decay that halts between 0.5 and 1 ps and then resumes decaying. The initial decay is attributed to Förster energy transfer while the latter is attributed to the increasing influence of the isotropic end spectrum (see also Figure 3).

transfer while the reorientation should be unaffected.

Results

Linear spectrum

From the linear spectra in Figure 1, we note that there is a large difference in the absorption cross-section between water and ice of the same temperature. Upon freezing, the central frequency of the O–H stretch mode shifts to the red, the absorption band becomes much narrower, and the total cross-section increases. The frequency of the O–H stretch mode is a direct measure of the strength of its donating hydrogen bond. The red shift in ice indicates that the hydrogen bond has become

stronger (leading to a weaker O–H chemical bond). The width of the spectrum is a measure of the amount of inhomogeneity present in the system. The fact that the spectrum narrows, shows that ice possesses a more homogeneous distribution of hydrogen bonds than water. A small inhomogeneity of the O–H stretch mode in ice Ih is caused by its inherent proton disorder. The spectrum thus reflects the fact that ice is more rigid and more structured than water. The increased cross-section is an indication that the O–H stretch mode has become more polarizable in ice.

Transient spectra

Figure 2 shows a typical data set of 15% H_2O with the frequency resolved (isotropic) absorption changes and anisotropy decays for various delay times between pump and probe. The isotropic spectra show part of the $\nu = 1 \rightarrow 2$ induced absorption, which extends between 2700 and 3300 cm^{-1}. We observe a rapid decay and a small (2%) thermalization end spectrum at delay times > 3 ps. This end spectrum shows a delayed ingrowth, indicative of an intermediate state between vibrational depopulation and thermalization. This intermediate state was previously shown[5] to have a blue-shifted spectrum that has no absorption cross-section in the current probe window. The total isotropic pump-probe signal, in this frequency region, can thus be described as the sum of a decaying vibrational spectrum $\sigma_1(\nu)$ and a delayed ingrowing thermalized end spectrum $\sigma_H(\nu)$:

$$\begin{aligned} \Delta\alpha(t,\nu) &= \sigma_1(\nu)\cdot\exp(-k_1\,t\,) \\ &+ \sigma_H(\nu)\cdot\left(\frac{k_1}{k^*-k_1}\exp(-k^*\,t\,) - \frac{k^*}{k^*-k_1}\exp(-k_1\,t\,)+1\right), \end{aligned} \tag{7}$$

where k_1 is the vibrational relaxation rate and k^* the thermalization rate.

The anisotropy data of Figure 2 show no significant frequency dependence. Within the first 500 fs the anisotropy drops to a value of about 0.18, where it stays for the next 500 fs. Finally it continues to drop down to zero where it stays for all times > 3 ps. From Eqs. 2 and 3 we can show that when the pump probe signal consists of multiple components that have different anisotropies, the total observed anisotropy at time t and frequency ν will be the average of the in-

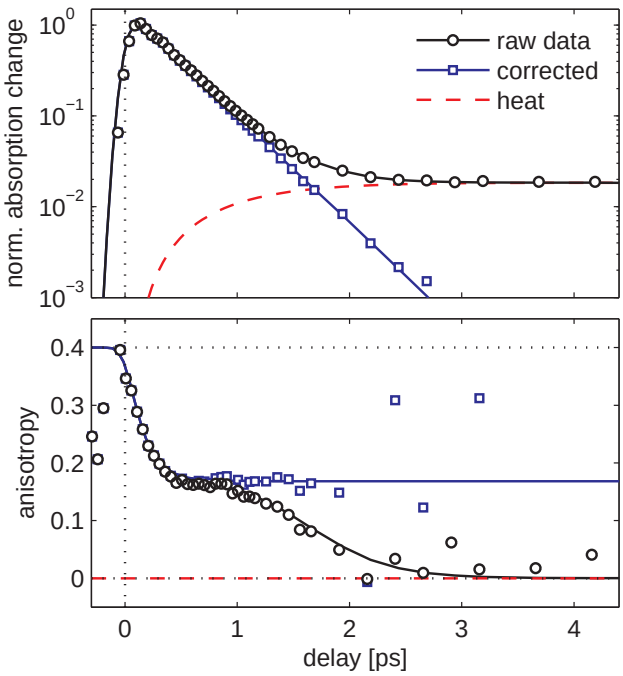

Figure 3: Frequency averaged isotropic (top) and anisotropic (bottom) signals of 15% H_2O ice. The circles indicate the raw data and the squares indicate the corrected data where an indirectly ingrowing isotropic heat (dashed line) has been subtracted (see text $\tau_1 = 350$ fs, $\tau^* = 600$ fs). The lines indicate the fitted model, which has been convoluted with an instrument response time of 200 fs.

dividual anisotropies $R_i(t)$, weighted with the (frequency dependent) isotropic intensities $\Delta\alpha_i(t,\nu)$:

$$R_{\text{total}} = \frac{\sum_i \Delta\alpha_i \cdot R_i}{\sum_i \Delta\alpha_i} = \frac{\Delta\alpha_1 \cdot R_1 + \Delta\alpha_H \cdot R_H}{\Delta\alpha_1 + \Delta\alpha_H}, \tag{8}$$

where R_1 is the (time dependent) anisotropy of the excited state ($\nu = 1$) that we are interested in, and R_H is the anisotropy of the thermalized end level.

Heat correction

To further analyze the data we take the weighted average of Figure 2 over all frequencies. The resulting time traces are shown in Figure 3 ('raw data'). The isotropic signal has been plotted logarithmically to show more clearly the initial exponential decay of the vibrational excitation,

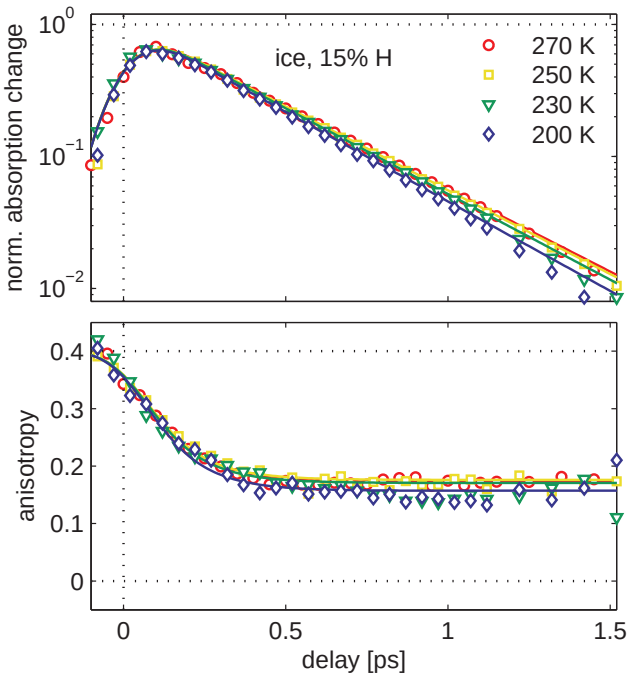

Figure 4: Isotropic and anisotropic signals of 15% H_2O ice at temperatures between 200 and 270 K. The data show minimal dependence on temperature with decay times τ_1 between 320 and 340 fs. The anisotropy end levels range between 0.16 and 0.18.

before the delayed ingrowth of the thermalization end level. Note that before the thermalization grows in, the anisotropy already shows a certain end level ($R = 0.18$). All fits are convoluted with the instrument response time of 200 fs:

The isotropic trace was fitted using Eq. 7, resulting in the rates $k_1 = 1/350$ fs^{-1} and $k^* = 1/600$ fs^{-1}. From the bottom part of Figure 2, we note that at later delay times (> 3 ps), where the thermalization signal is dominant, the signal becomes isotropic ($R = 0$). We therefore set R_H to zero, while leaving R_1 free. We proceed by subtracting the fitted thermalization parts ('heat') from the 'raw data' using Eqs. 7 and 8. The resulting traces are shown as 'corrected' data for both the isotropic and anisotropic parts. Note that the isotropic part of the corrected data shows a mono-exponential decay as expected from Eq. 7. The anisotropic corrected data shows a continuation of the end level at $R = 0.18$. Note from Eq. 3 that the anisotropy can only be accurately determined as long as the vibrational excitation persists, which is why the noise goes up beyond 2 ps.

Temperature dependence

Figure 4 shows heat-corrected and normalized data traces of 15% H_2O for temperatures between 200 and 270 K. We observe little temperature dependence, both in the isotropic and anisotropic data traces. The vibrational relaxation rate goes up very slightly with decreasing temperature (340→320 fs). The anisotropy traces show no clear temperature dependence, neither in the end levels (0.16–0.18), nor in the rate of the initial decay (∼140 fs). This temperature independence implies that all conclusions drawn from the data will be equally valid for all temperatures of hexagonal ice Ih between 200–270 K.

In a previous study on the reorientational diffusion of liquid water[19] (4% D_2O in H_2O), the anisotropy decay time constants decreased from 5 to 1 ps, for a temperature increase from 5 to 70°C (278–343 K), respectively. Also, the anisotropies decayed fully down to zero. Clearly the anisotropy decay observed in Figure 4 is of a completely different origin. Whereas the anisotropy decay in liquid (isotopically diluted) water is mainly caused by orientational diffusion (Eq. 5), the anisotropy decay in ice is mainly the result of vibrational Förster energy transfer (Eq. 6).

We assign the initial decay process with a time constant of ∼140 fs to Förster transfer between nearby O–H oscillators and the lack of decay after 0.5 ps to the absence of reorientational motion due to the restrictions of the ice crystal. Taking into account the noise of the end level and the short interval over which the anisotropy can be measured, the reorientational diffusion time τ_R of a water molecule in ice is estimated to be >15 ps. For all current purposes this means that the reorientational motion is 'frozen'. We note further that the presence of a nonzero end level is a clear indication that the Förster transfer radius in ice has a cutoff.

Concentration dependence

Figure 5 shows normalized and heat-corrected data for concentrations of f_H between 0.1 and 100%. To better show the difference in the isotropic signals (top), all data were divided by the mono-exponential fit to the lowest concentration (0.1%). This concentration of 0.1% is expected to be low enough to prevent vibrational Förster transfer between O–H groups.[20] From the resulting decay

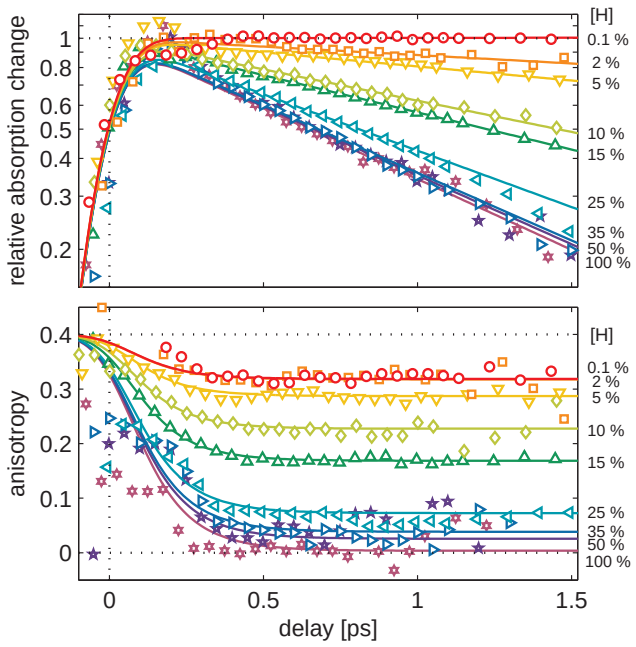

Figure 5: Heat corrected data and fits of all measured concentrations of H_2O in D_2O ice at 270 K. The isotropic data (top) has been divided by $\exp(2.2t)$ (i.e. the relaxation rate for 0.1% H_2O) to better show the effect of increasing H_2O concentrations. It may be noted that the additional relaxation channel is still mono-exponential, which means that the effect of adding H_2O is simply to increase the overall relaxation rate (from 2.2 up to 3.3 ps^{-1}). The anisotropy end levels show a clear decreasing trend indicative of Förster energy transfer between nearby O–H stretch vibrations as the H_2O concentration increases. For 100% H_2O we observe complete isotropic redistribution. The lines in the top figure indicate mono exponential fits to the data while for the bottom figure they show exponentials decaying to an end level. In both cases the fits were convoluted with the instrument response time (200 fs). Data points for delay times < 200 fs are affected by coherent artifacts.

traces it is clear that increasing f_H results in an additional *mono-exponential* relaxation channel. All isotropic data can be described with:

$$\Delta\alpha(t) \;=\; \exp\left[-\left(k_0+\Delta k(f_H)\right)\,t\right], \tag{9}$$

where $k_0 = 1/450\ \mathrm{fs}^{-1}$ is the rate of decay of $f_H = 0.1\%$ and $\Delta k(f_H)$ is the concentration dependent additional. The fitted decay rates $k_0+\Delta k(f_H)$ are summarized in Figure 6. The decay rate goes up quickly for the initial concentration increases but levels off beyond 35%.

Next, we examine the anisotropic data of Figure 5 (bottom). We note that all traces exhibit a

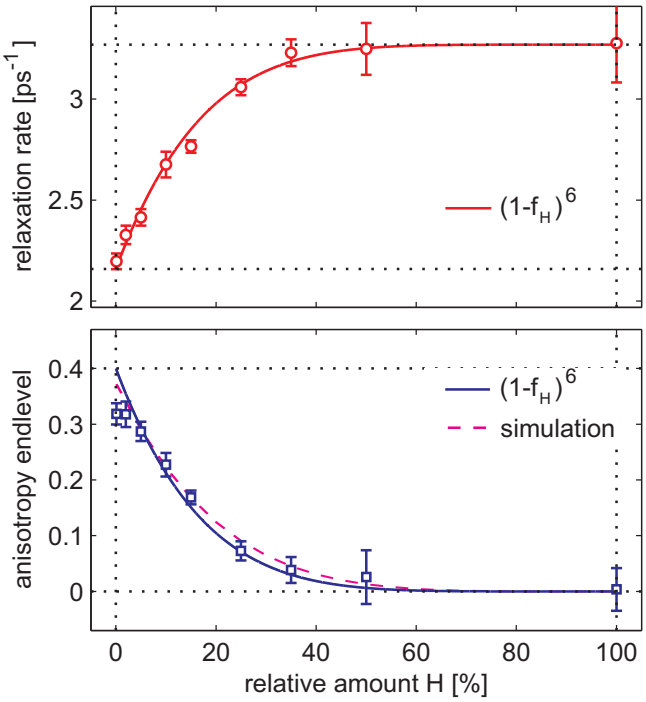

Figure 6: Relaxation rates $k_0 + \Delta k(f_H)$ and anisotropy end levels $E(f_H)$ for all concentrations of H_2O in D_2O ice at 270 K. The lines show that both data closely follow the trend $(1 - f_H)^6$, where f_H is the fraction of H_2O in the sample. This can be interpreted as meaning that both the rate increase and the anisotropy end level is dependent on the proximity of at least one hydrogen in its (nearest) six neighbors.

similar rapid initial decay to a clear and distinct end level. These traces can be fitted well:

$$R(t) \;=\; E(f_H) + [0.4 - E(f_H)] \cdot \exp\left(-k_F\, t\right), \tag{10}$$

where $k_F = 1/140$ fs^{-1} is the decay rate and $E(f_H)$ is the concentration dependent end level. The resulting fitted end levels are summarized in Figure 6. The end levels drop significantly when the concentration is increased from 5% to about 35%.

Ice structure

Comparing the top and bottom panels of Figure 6, we observe a strong similarity between the increase of the isotropic decay rate and the drop in the end levels of the anisotropy. This observation

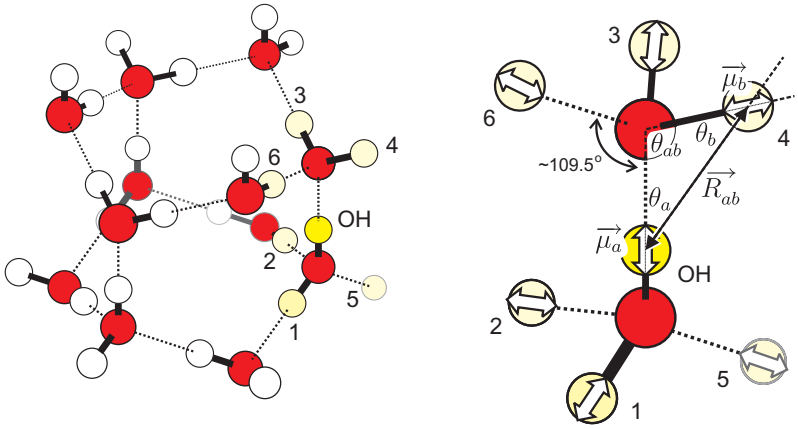

Figure 7: Three dimensional structure of hexagonal ice (c-axis vertical) showing the excited O–H stretch vibration and the nearest six hydrogen atoms. The solid lines indicate covalent bonds while the dashed lines indicate hydrogen bonds. The white arrows indicate the direction of the transition dipole moments of the O–H or O–D stretch vibrations.

indicates that a similar cause may be at the root of both phenomena.

The decrease of the end levels of the anisotropy is directly related to the increased chance for vibrational Förster transfer between neighboring O–H groups. To get an idea about the effects of vibrational energy transfer on the anisotropy, we examine more closely the structure of ice Ih in Figure 9. This figure shows part of a hexagonal ice crystal, where the oxygen atoms are arranged according to the $P6_3/mmc$ space group,[1,21] and are surrounded tetrahedrally by hydrogen atoms according to the Bernal-Fowler ice rules.[2] We set the covalent O–H distance to 1.0 Å and the hydrogen bond O···H distance to 1.8 Å in accordance with neutron and x-ray diffraction studies on ice.[22] Finally, in accordance with a study by Buch and Devlin,[23] we will assume that the direction and position of the transition dipole moment lie along the O–H bond of the water molecule at 0.65 Å from the oxygen atom.

Förster rate

The rate of vibrational energy transfer k_F between two dipole oscillators a and b is described by the Förster expression:[24,25]

$$k_{F,ab} \sim \frac{|\mu_a|^2|\mu_b|^2\kappa_{ab}^2}{|R_{ab}|^6}\int \sigma_a(\nu)\sigma_b(\nu)\,d\nu\,, \tag{11}$$

where μ_a and μ_a are the transition dipole moments of the transmitting and receiving dipole modes, R_{ab} is the distance between the dipoles, σ_a and σ_b are the normalized vibrational line shapes of the two modes, and κ_{ab} is a geometrical factor expressing the relative orientations of the dipole moments (see Figure 9):

$$\kappa_{ab} = \hat{\mu}_a\cdot\hat{\mu}_b - 3(\hat{\mu}_a\cdot\hat{R}_{ab})(\hat{\mu}_a\cdot\hat{R}_{ab}) \approx \cos\theta_{ab} + 3\cos\theta_a\cos\theta_b\,, \tag{12}$$

where the hats denote normalized unit vectors. The latter equality only holds if all vectors lie in a plane along a triangle as drawn in Figure 9, i.e. the transition dipoles point along the O–H$\cdots$O bonds.

The overlap integral between $\sigma_a(\nu)$ and $\sigma_b(\nu)$ is virtually zero for an O–H vibration transferring to an O–D vibration due to the frequency mismatch. This means that the O–H vibration will only be dipole coupled to other O–H groups. We take the dipole strengths μ of different oscillators to be uniform in the ice crystal as is corroborated by the more homogeneous spectrum in Figure 1.

The regular structure and angles of the ice crystal lead to well-defined geometrical factors κ_{ab}. For example, we see from Figure 9 that the neighboring O–H groups are all oriented with angles close to $\theta_a \approx \theta_b \approx 35^\circ$. This leads to a similar orientational factor for these neighbors (all $\kappa_{ab} \approx 1.6 \pm 0.1$). The main factor to consider in the estimation of the Förster coupling strength is thus the distance R_{ab} between O–H oscillators (i.e. the distance between hydrogen atoms).

For atom 1, which is the hydrogen that is part of the same water molecule, this distance is the smallest: $R_{OH,1} \approx 1.6$ Å. The next four closest hydrogen atoms are those on the neighboring

water molecules (atoms 2-5), all with a distance of ∼2.3 Å, followed by atom 6 which donates a hydrogen bond to the same oxygen as the excited O–H ($R_{OH,6} \approx 2.9$ Å). We note that for any configuration according to the Bernal-Fowler ice rules,[2] there will always exist these six closest neighbors in the hexagonal ice lattice. Beyond these six, the next nearest neighbor, is at a distance of ∼3.6 Å and possesses a lower geometrical factor $\kappa_{ab} \approx 0.9$.

Limited transfer range

Table 1: **Förster parameters**

atom	κ_{ab}	R_{ab}	κ_{ab}^2/R_{ab}^6
1	1.6	1.1	1.4
2-5	1.6	2.4	1.3×10^{-2}
6	1.6	3.2	2.4×10^{-3}
2nd shell	0.9	3.9	2.3×10^{-4}

The distance and geometrical information is summarized in Table 1, together with the resulting influence on the Förster transfer rate according to Eq. 11. We note that this rate quickly diminishes by about an order of magnitude for each next neighbor. We now speculate that this strong distance dependence, together with the highly ordered structure of ice is the reason for the clearly different time-regimes of the rapid initial drop in end-level and the subsequent much slower decay.

Model

Let us assume that the presence of a sufficiently nearby O–H to the original excitation will lead to a decay of the anisotropy. Or inversely, if no nearby O–H exists, the anisotropy will not decay. The measured anisotropy end-level will be the average over all possible configuration of hydrogen and deuterium. As a simple approach we consider the chance p that the nearest N atoms, to which Förster transfer can take place, are all deuterium. This chance is dependent on the fraction of hydrogen f_H as:

$$p(f_H) \;=\; (1 - f_H)^N . \tag{13}$$

This will also be the fraction of excited O–H oscillators that cannot Förster transfer their vibrational energy to any nearby neighbor and will keep their original orientation. As we have seen in Eq. 8, the total anisotropy end level is the average over all configurations. If we assume, for simplicity, that if no transfer can take place the anisotropy remains $R = 0.4$, while any transfer leads to an anisotropy $R = 0$, the end level E will be given simply by:

$$E(f_H) \;=\; 0.4 \cdot (1 - f_H)^N . \tag{14}$$

We fit this simple model to the data in Figure 6, and find that the data can be best described using a value of N between 5 and 6. This number indicates that the O–H vibration is Förster coupled to at most six of its nearest neighbors, and negligible beyond. Basically, the steepness of the end level decrease has to agree with the number of contributing neighbors. If only the nearest neighbor (of the same water molecule) were involved, a linear dependence ($N = 1$) would have been found. Conversely, if more than six neighbors were involved, the end level would have dropped more rapidly.

We note finally that although the vibrational relaxation is well described by the current model (top panel Figure 6), the description of the anisotropy end level deviates somewhat for the lowest concentrations $f_H < 2\%$ (bottom panel Figure 6). We observe that even for the lowest concentration $f_H = 0.1\%$, the anisotropy end level does not remain at 0.4. The most likely explanation for this observation is, that the direction of the transition dipole moments in the ice crystal is not completely static, even though no (complete) reorientation of the water molecules takes place. This phenomenon has been previously observed in the initial rapid anisotropy decay of liquid water and was interpreted as a 'librational cone'.[26] This effect is of less importance if the vibrational energy can jump to another O–H group, since it only tends to lower the overall anisotropy. From Eq. 5 we may deduce that the observed end level of $R = 0.33$ would correspond to a librational cone angle of about $\sim 20^\circ$.

Förster radius

The distance dependent Förster rate $k_F(R)$ can be calculated using the following formula:

$$k_F(R) \;=\; \frac{1}{\tau_1}\left(\frac{R_0}{R}\right)^6, \tag{15}$$

where R is the distance between donor and acceptor, τ_1 is the donor lifetime, and R_0 is the Förster radius defined as the distance where $k_F(R_0) = 1/\tau_1$. Using Eq. 15 we first calculate the Förster radius of the O–H vibration in ice. We fill in $\tau_1 = 0.45$ ps, the vibrational lifetime of $f_H = 0.1\%$, and $k_F(R) = 1/140$ fs^{-1} for a transfer to the nearest neighbors (atoms 2-5) at a distance $R = 2.3$ Å (see Table 1). This results in a radius $R_{0,\mathrm{OH(s)}} = 2.8$ Å.

This radius is bigger than those previously found for the O–H in liquid D_2O[16] ($R_{0,\mathrm{OH}(\ell)} = 2.1$ Å) and the O–D in liquid H_2O[20] ($R_{0,\mathrm{OD}(\ell)} = 2.3$ Å). To compare the rates of Förster transfer between liquid water and ice we use Eq. 15 to derive:

$$\hat{k}_F \;\equiv\; k_F(R)\times R^6 \;=\; \frac{R_0^6}{\tau_1}, \tag{16}$$

where $\hat{k}_F$ is the normalized Förster rate for $R = 1$. Filling in the lifetime and Förster radius of the O–H vibration in ice results in $\hat{k}_{F,\mathrm{OH(s)}} = 1.1\times10^3$ ps^{-1} Å^6. For the O–H vibration in liquid water we use $\tau_1 = 0.7$ ps[15] and calculate $\hat{k}_{F,\mathrm{OH(l)}} = 1.2\times10^2$ ps^{-1} Å^6. So we find that the Förster rate in ice is almost ten times higher than in liquid water. We note that these two rates were derived using quite different methods. The rate in liquid water was derived from a fit to a continuum model,[16] while the currently found rate in ice was estimated from the (single) discrete rate to the closest neighbors.

A previous study,[20] comparing the Förster rates of the O–H and O–D stretch vibrations in liquid water, found that the differences in transfer rates ($\hat{k}_{F,\mathrm{OH(l)}} \approx 2.3\,\hat{k}_{F,\mathrm{OD(l)}}$) could be explained from the differences in the linear absorption spectra, i.e. the differences in transition dipole strength. We have already seen in Figure 1 that the absorption cross-section of ice is much higher than that

of liquid water, thus explaining at least part of the increased Förster rate. Another part could be explained by looking at the difference in the shape of the absorption spectra. We note in Figure 1 that the absorption line shape of liquid water (i.e. gaussian) indicates a significant amount of inhomogeneous broadening, whereas the absorption line shape of ice looks much more like a Lorentzian (indicative of homogeneous broadening). Because the O–H stretch modes in ice are more homogeneous than in liquid water, the average absorption and emission spectra in ice will also be very similar and thus better overlapped. As can be seen from the overlap integral in Eq. 11, an enhanced frequency overlap between donor and acceptor leads to an enhanced Förster rate.

From Table 1 we note that the expected rate of Förster transfer to the first O–H groups outside of the 6 closest neighbors is 10 times slower than to atom 6 and 56 times slower than to atoms 2–5. This large gap in coupling strength could explain why we do not notice the influence of hydrogen atoms beyond those of the closest six neighbors. If we assume the rate of Förster transfer to atoms 2–5 to be 1/140 fs^{-1}, the rate to O–H groups beyond atom 6 (2^{nd} shell) would be on a time scale > 7.8 ps. This explains why we see a plateau in the anisotropy decay: after the initial rapid transfer to the nearest neighbors has taken place, the rate to the next neighbors is too slow to observe in a picosecond time window.

A major difference between liquid water and ice is the amount of inhomogeneity. Whereas in liquid water there exist a wide variety of different hydrogen bond angles, distances and strengths, the water molecules in ice are much more rigidly positioned. That is why we do not observe a continuous distance dependence in ice. Of course, for water such a continuum description will also break down for transfer distances comparable to the molecular size, but because the anisotropy decay in water also involves the molecular reorientation, such effects are less noticeable than in ice.

Cluster simulation

Several assumptions were made in the simplified model of Eq. 14. To check the justification of these assumptions we perform a set of simulations that more accurately reflect the physical layout

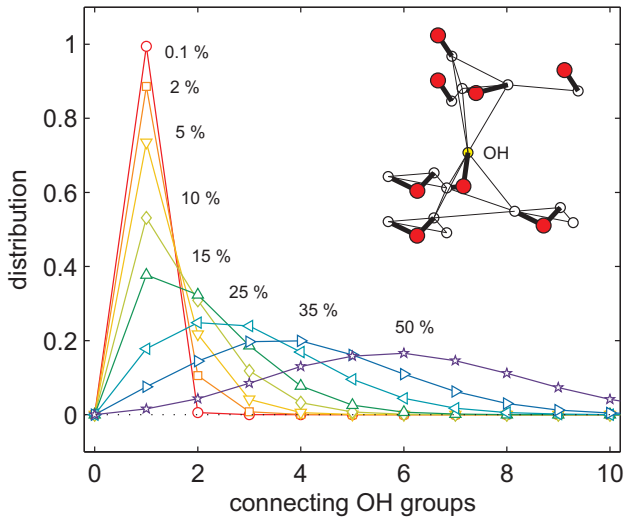

Figure 8: Distribution of the number of (consecutively) neighboring O–H groups (H–H distance < 3 Å) in H_2O/D_2O hexagonal ice as a function of H_2O concentration. The top-right inset shows an example cluster where thin lines connect each hydrogen atom to its closest neighbors.

(i.e. orientations and positions) of the O–H stretch oscillators in the hexagonal ice lattice.

For the simulation we use a series of randomly generated hexagonal ice crystals. Starting from a central hydrogen atom, we use configurations of up to 20 nearest neighbors and loop over all possible 2^{20} configurations of hydrogen and deuterium atoms. Within each configuration we determine the cluster of (consecutively) neighboring O–H groups, where a connection is defined as $R_{H-H} < 3$ Å (six nearest, see Table 1). Figure 8 shows an example cluster and the distribution of close O–H groups for different concentrations that were used. From this figure we note that for concentrations up to 15%, the dominant configuration consists of a set of two neighboring O–H groups and that the number of neighboring O–H groups remains finite for concentrations up to 50%.

We allow the vibrational excitation to randomly hop to any hydrogen within the interconnecting cluster (multiple hops allowed) and record the relative angles of the transition dipole moments, with respect to the original excitation (assuming they lie along the O–H bond). Using Eq. 6 we proceed to calculate the corresponding anisotropies of the individual O–H groups. These individual anisotropies are averaged to yield the anisotropy of the cluster. These cluster anisotropies are

weighted with the chance of that particular cluster occurring, finally yielding the total anisotropy (end level). The result of this simulation is shown as the dashed line in Figure 6. It shows good agreement with both the data and the simple model described in Eq. 14.

Vibrational relaxation rate

We now turn our attention to the concentration dependent vibrational relaxation rate, recorded in Figure 6. As we noted before, the trend of the increasing relaxation rate is very similar to that of the anisotropy end level, which means they are likely caused by the same phenomenon. Indeed we see in Figure 6 that we may fit the vibrational relaxation time quite nicely using:

$$\Delta k(f_H) \;=\; \Delta k_{\max} \cdot \left[1-(1-f_H)^N\right], \tag{17}$$

where $\Delta k_{\max} = 1.1$ ps^{-1} is the maximum rate increase observed for a concentration of $f_H = 100\%$.

The origin of the concentration dependence of the anisotropy end level was established as the proximity of at least one hydrogen atom in one of the six nearest neighbors. We note that the Förster transfer of a vibrational excitation does not lead to the decay of that excitation, but only to a displacement (and different direction). The local density of accepting modes may be different after this displacement, but not necessarily higher. So this displacement need not necessarily lead to an enhanced relaxation of the O–H stretch mode. We therefore need to look for the effect of a nearby hydrogen atom on any of the possible accepting modes of the O–H stretch.

To understand the nature of this additional channel it is useful to first determine the principal relaxation channel for the O–H stretch mode in ice. From a previous study[5] on 2.5% H_2O in D_2O ice Ih, it was observed (in agreement with our current findings) that the relaxation proceeds through an intermediate level, before manifesting as a thermalized end spectrum. Also, the relaxation time that was found in that study (420 fs) is in excellent agreement with the current results (cf. $f_H = 2.5\%$ in Figure 6). It was noted,[5] that the anisotropy of the intermediate level did not deviate from that of the $\nu = 0 \rightarrow 1$ transition. This leads to the conclusion that the intermediate level

consists of a mode that is located nearby the original excitation. Finally, the intermediate level has an associated spectrum that is wider and blue-shifted compared to the $v = 0 \rightarrow 1$ transition. This blue-shift can be caused both as a result of a weakened hydrogen bond or as the result of an anharmonic coupling between the O–H stretch mode and the H–O–D bending mode.[4]

For the observed rate increase, we note that replacing a deuterium atom in HOD with a hydrogen atom, will affect its bending mode and improve the coupling strength to the O–H stretch mode. However, the additional relaxation increases with a trend that suggest it is facilitated by the presence of hydrogen in one of *six* nearby neighbors. If it were only influenced by the hydrogen present in the same molecule, we would have found a linear concentration dependence. These observations indicate that *also* intermolecular coupling must play a role in the current observations. We speculate that the *additional* relaxation channel consists of the coupling between the O–H stretch mode and a combination of two H–O–D bending modes on two neighboring water molecules. A similar relaxation path, where the energy of the O–H stretch was redistributed over the H–O–H bending modes of two water molecules was previously observed for the vibrational relaxation of pure liquid water.[4]

Conclusion

We have measured the relaxation time and anisotropy decay of the O–H stretch vibration in ice Ih for a range of temperatures and ratios H_2O/D_2O. We used a model with an intermediate level to correct for the effects of the (isotropic) thermalization dynamics on the relaxation and anisotropy. For increasing concentrations of H_2O, we find that the vibrational relaxation time decreases from 480 fs (0.1%) down to 300 fs (100%), and that the anisotropy end level decreases from $\sim$0.33 (0.1%) to 0 (100%). The initial decrease in the anisotropy level from 0.4 to 0.33 is interpreted as the result of the librational motion of the water molecules over a cone of $\sim 20^\circ$. The subsequent $\sim$140 fs decay of anisotropy is attributed to vibrational Förster energy transfer to nearby O–H stretch modes.

We observe the relaxation rate to become slightly faster ($\sim$5%) when the temperature is decreased from 270 to 200 K. The concentration dependence of the anisotropy end level and the relaxation rate can be modeled (phenomenologically) assuming a $(1 - f_H)^6$ dependence on the fraction of hydrogen atoms f_H. The exponent is interpreted as the influence of the six nearest neighboring hydrogen atoms. The strong cut-off between these six neighbors and those further away is caused by a combination of the strong $1/R^6$ distance dependence of the dipole-dipole (Förster) coupling and the discrete character of the distances between atoms in the ice crystal.

This phenomenological model was checked using a set of (cluster) simulations that contained a more complete description of the exact structure and distances in hexagonal ice. For ice there exists a discrete set of distances where the dipolar coupling of the neighbors in the second shell is about two orders of magnitude less than those of the nearest neighbors in the first shell. This picture contrasts with the continuum description of Förster transfer in liquid water. The strong correlation of the concentration dependence of the relaxation rate with the Förster energy transfer indicates that the hopping between O–H oscillators helps in finding a vibrational relaxation pathway.

Acknowledgement

This work is part of the research program of the Foundation for Fundamental Research on Matter (FOM) which is financially supported by the Dutch organization for Scientific Research (NWO). The authors thank Hinco Schoenmaker for his technical support.

References

(1) Morrison, I.; Li, J.; Jenkins, S.; Xantheas, S.; Payne, M. *J. Phys. Chem. B* **1997**, *101*, 6146–6150.

(2) Bernal, J. D.; Fowler, R. H. *J. Chem. Phys* **1933**, *1*, 515–548.

(3) Woutersen, S.; Emmerichs, U.; Nienhuys, H.-K.; Bakker, H. J. *Phys. Rev. Lett.* **1998**, *81*, 1106–1109.

(4) Lindner, J.; Vohringer, P.; pshenichnikov, M. S.; Cringus, D.; Wiersma, D. A.; Mostovoy, M. *Chem. Phys. Lett* **2006**, *421*, 329–333.

(5) Dokter, A. M.; Bakker, H. J. *J. Chem. Phys* **2008**, *128*, 024502.

(6) Lawrence, C. P.; Skinner, J. L. *J. Chem. Phys* **2003**, *118*, 264–272.

(7) Auer, B.; Kumar, R.; Schmidt, J. R.; Skinner, J. L. *PNAS* **2007**, *104*, 14215–14220.

(8) Förster, T. *Ann. Physik* **1948**, *2*, 55–75.

(9) Graener, H.; Seifert, G.; Laubereau, A. *Chem. Phys.* **1993**, *175*, 193–204.

(10) Nienhuys, H.-K.; Van Santen, R. A.; Bakker, H. J. *J. Chem. Phys* **2000**, *112*, 8487–8494.

(11) Stenger, J.; Madsen, D.; Hamm, P.; Nibbering, E. T. J.; Elsaesser, T. *Phys. Rev. Lett.* **2001**, *87*, 027401.

(12) Gallot, G.; Bratos, S.; Pommeret, S.; Lascoux, N.; Leicknam, J. C.; Kozinski, M.; Amir, W.; Gale, G. M. *J. Chem. Phys* **2002**, *117*, 11301–11309.

(13) Asbury, J. B.; Steinel, T.; Kwak, K.; Corcelli, S. A.; Lawrence, C. P.; Skinner, J. L.; Fayer, M. D. *J. Chem. Phys* **2004**, *121*, 12431–12446.

(14) Eaves, J. D.; Loparo, J. J.; Fecko, C. J.; Roberts, S. T.; Tokmakoff, A.; Geissler, P. L. *PNAS* **2005**, *102*, 13019–13022.

(15) Rezus, Y. L. A.; Bakker, H. J. *J. Chem. Phys* **2006**, *125*, 144512.

(16) Woutersen, S.; Bakker, H. J. *Nature* **1999**, *402*, 507–509.

(17) Cowan, M. L.; Bruner, B. D.; Huse, N.; Dwyer, J. R.; Chugh, B.; Nibbering, E. T. J.; Elsaesser, T.; Miller, R. J. D. *Nature* **2005**, *434*, 199.

(18) Lipari, G.; Szabo, A. *Biophys. J.* **1980**, *30*, 489–506.

(19) Tielrooij, K.; Petersen, C.; Rezus, Y.; Bakker, H. *Chem. Phys. Lett* **2009**, *471*, 71 – 74.

(20) Piatkowski, L.; Eisenthal, K. B.; Bakker, H. J. *Phys. Chem. Chem. Phys.* **2009**, *11*, 9033–9038.

(21) Bjerrum, N. *Kong. Danske Vid. Selsk. mat.-fys. Medd.* **1951**, *27*, 56.

(22) Isaacs, E.; Shukla, A.; Platzman, P.; Hamann, D.; Barbiellini, B.; Tulk, C. *Phys. Rev. Lett.* **1999**, *82*, 600–603.

(23) Buch, V.; Devlin, J. P. *J. Chem. Phys* **1999**, *110*, 3437–3443.

(24) Morin, M.; Jakob, P.; Levinos, N. J.; Chabal, Y. J.; Harris, A. L. *J. Chem. Phys* **1992**, *96*, 6203–6212.

(25) Woutersen, S.; Emmerichs, U.; Bakker, H. J. *J. Chem. Phys* **1997**, *107*, 1483–1490.

(26) Fecko, C. J.; Loparo, J. J.; Roberts, S. T.; Tokmakoff, A. *J. Chem. Phys* **2005**, *122*, 054506.

Table of Contents graphic

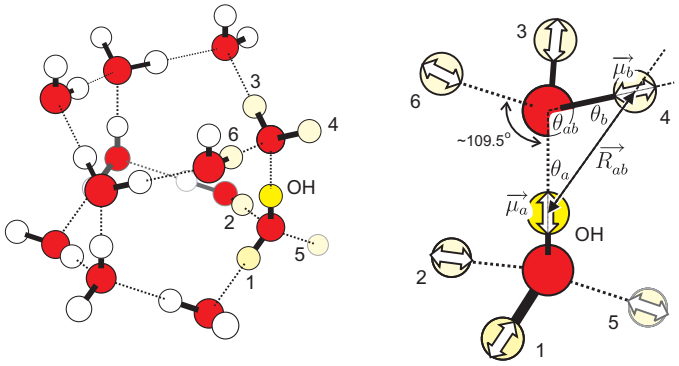

Figure 9: Three dimensional structure of hexagonal ice (c-axis vertical) showing the excited O–H stretch vibration and the nearest six hydrogen atoms. The solid lines indicate covalent bonds while the dashed lines indicate hydrogen bonds. The white arrows indicate the direction of the transition dipole moments of the O–H or O–D stretch vibrations.